JOURNAL OF VIROLOGY, June 2008, p. 5703–5714 Vol. 82, No. 12
0022-538X/08/$08.00+0 doi:10.1128/JVI.02760-07

Functional and Structural Dynamics of Hepadnavirus Reverse Transcriptase during Protein-Primed Initiation of Reverse Transcription: Effects of Metal Ions▽

Li Lin, Fen Wan, and Jianming Hu*

Department of Microbiology and Immunology, The Pennsylvania State University College of Medicine, Hershey, Pennsylvania 17033

Received 28 December 2007/Accepted 2 April 2008

Reverse transcription in hepadnaviruses is primed by the viral reverse transcriptase (RT) (protein priming) and requires the interaction between the RT and a specific viral RNA template termed ε. Protein priming is resistant to a number of RT inhibitors that can block subsequent viral DNA elongation and likely requires a distinct "priming" conformation. Furthermore, protein priming may consist of two distinct stages, i.e., the attachment of the first deoxynucleotide to RT (initiation) and the subsequent addition of 2 or 3 deoxynucleotides (polymerization). In particular, a truncated duck hepatitis B virus RT (MiniRT2) is competent in initiation but defective in polymerization when tested in the presence of Mg^{2+}. Given the known effects of metal ions on the activities of various DNA and RNA polymerases, we tested if metal ions could affect hepadnavirus RT priming. We report here that Mn^{2+}, in comparison with Mg^{2+}, showed dramatic effects on the priming activity of MiniRT2 as well as the full-length RT. First and foremost, MiniRT2 exhibited full polymerization activity in the presence of Mn^{2+}, indicating that MiniRT2 contains all sequences essential for polymerization but is unable to transition from initiation to polymerization with Mg^{2+}. Second, the initiation activities of MiniRT2 and the full-length RT were much stronger with Mn^{2+}. Third, the nucleotide and template specificities during protein priming were decreased in the presence of Mn^{2+}. Fourth, polymerization was sensitive to inhibition by a pyrophosphate analog in the presence of Mn^{2+} but not in the presence of Mg^{2+}. Finally, limited proteolysis provided direct evidence that the priming active MiniRT2 adopted distinct conformations depending on the presence of Mn^{2+} versus that of Mg^{2+} and that the transition from initiation to polymerization was accompanied by RT conformational change.

Hepadnaviruses (hepatitis B viruses [HBVs]) are retroid viruses that replicate a small (ca. 3-kb) DNA genome via an RNA intermediate, the pregenomic RNA (pgRNA). The hepadnavirus reverse transcription pathway shows both similarities to and differences from that of classical retroviruses, including the mechanisms of nucleocapsid assembly and the initiation of DNA synthesis (40, 42, 45). To carry out their unique life cycle, the hepadnaviruses encode a specialized reverse transcriptase (RT) protein that displays a number of unique properties distinct from those of its retrovirus counterparts (23). Chief among these is its ability to initiate DNA synthesis de novo without the help of any DNA or RNA primer. Instead, a specific tyrosine residue within RT itself is used as the primer to initiate viral minus strand DNA synthesis (the so-called protein priming reaction) (31, 32, 52, 53, 56, 58).

The unique ability of the hepadnavirus RT to carry out protein priming by using itself as a protein primer is reflected in its novel structural organization (11, 22, 23, 37). RT consists of four domains: from the N to the C terminus, they are the terminal protein (TP), the spacer, the RT, and the RNase H domains. TP is conserved among all hepadnaviruses but absent from any other known proteins. It is within TP where the aforementioned primer tyrosine residue is located. The functionally dispensable spacer connects TP to the central RT domain. Both the RT and RNase H domains share sequence homology with conventional RTs, including the YMDD active site motif in the RT domain and the catalytic D residues in the RNase H domain. Based on sequence alignment, structure modeling, and some genetic and biochemical data, the RT domain can be further divided into the finger, palm, and thumb subdomains, as in virtually all DNA and RNA polymerases (14, 41).

Although no viral protein other than RT itself is required for protein priming in hepadnaviruses, there is an absolute requirement for a specific RNA template, the short RNA stem-loop structure, called ε, located on pgRNA (36, 53). The ε RNA bears two inverted repeat sequences and can fold into a conserved stem-loop structure, with a lower and an upper stem, an apical loop, and an internal bulge (16, 17, 22, 25, 28). Using the internal bulge of ε as the obligatory template and the specific tyrosine residue within its TP domain as the protein primer, RT synthesizes a 3- to 4-nucleotide (nt)-long DNA oligomer that is covalently attached to RT through the tyrosine residue (52, 53). Following the synthesis of this short DNA oligomer, the nascent DNA-RT complex is translocated from ε to an acceptor site near the 3′ end of pgRNA, from which reverse transcription continues (1, 2, 49, 51). Rather than serving simply as a passive template for protein priming, ε plays an active role in stimulating the enzymatic function of RT by inducing conformational changes in the latter (47, 48) while also undergoing significant conformational changes itself upon binding to RT (8, 10). Thus, a functional ribonucleoprotein (RNP) complex that is active in protein priming is formed only

* Corresponding author. Mailing address: Department of Microbiology and Immunology, H107, The Penn State University College of Medicine, 500 University Dr., Hershey, PA 17033. Phone: (717) 531-6523. Fax: (717) 531-6522. E-mail: juh13@psu.edu.

▽ Published ahead of print on 9 April 2008.

after both RT and ε undergo structural changes via an induced-fit mechanism. Adding to the importance of RT-ε interaction in hepadnavirus replication is its absolute requirement in packaging both RT and pgRNA into replication-competent nucleocapsids (4, 6, 18), where most, if not all, viral DNA synthesis occurs.

As only a single hepadnavirus RT molecule is believed to be packaged into the viral nucleocapsid (5, 57) and thus able to carry out the complete synthesis of the viral DNA following nucleocapsid assembly, it seems plausible that a single RT polypeptide can serve both as the primer and as the catalyst for DNA synthesis. This is in contrast to other known protein priming reactions, where the protein primer and the DNA or RNA polymerase activity reside on separate polypeptides (e.g., in adenoviruses and picornaviruses) (39). As a result of this unique protein priming mechanism, RT remains covalently attached to the 5′ end of the viral minus strand DNA during the entire process of reverse transcription. The direct physical linkage of the primer and the catalyst likely imposes considerable constraint on the RT structure as it carries out protein priming and the subsequent series of reactions to produce the characteristic, partially double-stranded, relaxed circular DNA from the single-stranded pgRNA template. The intricate conformational gymnastics that RT likely undergoes during these complex reactions, and the additional factors likely involved, are poorly understood at present due to the dynamic nature of these processes and a lack of any high-resolution RT structures.

Recent success in reconstituting hepadnavirus protein priming under cell-free and chemically defined conditions has provided experimentally tractable systems for elucidating the requirements for and the mechanisms of this complex reaction. In particular, a cellular chaperone complex consisting of heat shock protein 90 (Hsp90) and its cofactors (Hsp70, Hsp40, Hop, and p23) has been identified as a critical host factor required for protein priming by helping to establish and maintain an RT conformation competent for ε binding and protein priming (7, 20, 21, 24, 26, 27, 43). Interestingly, by removing the N-terminal third of TP, most of the spacer, part of the RT domain (the putative thumb subdomain), and the entire RNase H domain, we have recently isolated a truncated RT protein from the duck HBV (DHBV), MiniRT2, which no longer strictly depends on the host chaperones for protein priming (55). Strikingly, MiniRT2 is able to initiate protein priming by covalently attaching the first nucleotide (dGMP) to the primer tyrosine residue in TP but is unable to carry out any additional DNA synthesis to complete protein priming (54). This result suggests that protein priming can be further divided into two distinct steps: the covalent attachment of the first nucleotide to RT (initiation) and the subsequent addition of 2 or 3 nt to the initiating nucleotide (polymerization). The failure of MiniRT2 to carry out polymerization suggests either that it lacks the necessary sequences required for this step of protein priming or that an RT conformational change, which MiniRT2 fails to undergo, has to occur for the transition from initiation to polymerization during protein priming.

Virtually all DNA and RNA polymerases require a divalent metal ion for catalysis, the choice of which is known to affect polymerase activities significantly (3, 12, 29, 35, 38, 50). We have tested potential effects of metal ions on hepadnavirus RT functions and report here that the choice of metal ions, Mn^{2+} versus Mg^{2+}, had dramatic effects on protein priming by MiniRT2 and the full-length DHBV RT as well. Most dramatically, the presence of Mn^{2+}, in contrast to that of Mg^{2+}, allowed MiniRT2 to transition from the initiation to the polymerization stage of protein priming. The metal ions also affected the protein priming efficiency, the selection of nucleotide substrates, the template requirement, and the sensitivity of the protein priming reaction to a pyrophosphate analog RT inhibitor. The multiple effects of the metal ions on protein priming were most likely mediated by RT structural differences induced by the different ions, as revealed by the differential protease digestion patterns.

MATERIALS AND METHODS

Plasmids. pcDNA-MiniRT2 and pGEX-MiniRT2 express the truncated DHBV RT protein, MiniRT2, and its glutathione *S*-transferase (GST) fusion, respectively, as described before (20). pSP64pA-DP expresses the full-length DHBV RT from the SP6 promoter in the pSP64pA vector. pGEX-TP and pGEX-RT express the DHBV TP (residues 75 to 220) and DHBV RT (residues 349 to 575) domain sequences, respectively, fused to GST, and were derived from pGEX-MiniRT2 by removing the RT and TP sequences, respectively (33).

Protein expression and purification. GST-MiniRT2, GST-TP, and GST-RT were expressed in the BL21-CodonPlus-RIL cells and purified using the glutathione resin, as previously described (20, 21). In vitro expression of the full-length DHBV RT and the truncated MiniRT2 protein, from pSP64pA-DP and pcDNA-MiniRT2, respectively, was carried out using the TNT-coupled rabbit reticulocyte lysate (RRL) system (Promega) as previously described (20, 24, 52) with minor modifications. Briefly, RT proteins were translated together with ε RNA (1 μM) at 30°C for 90 min. Following translation, the reaction mixture was desalted by passing it through a Sephadex G-50 spin column (Roche) twice to remove endogenous deoxynucleoside triphosphates (dNTPs), Mg^{2+}, and other small molecules. The desalted RRL containing the translated RT proteins was then used for protein priming. MiniRT2/BstE was also expressed similarly by in vitro translation in RRL after linearizing pcDNA-MiniRT2 with BstE II, which cleaves the MiniRT2 sequence at codon 561, leading to an additional 14-residue truncation from the C terminus of MiniRT2. The luciferase was translated in RRL and desalted before being used for protease digestion.

RNA templates. A minimal DHBV ε RNA (44 nt long, from nt 2566 to 2609) (20) was used as the wild-type ε RNA throughout this study. The UUAU ε mutant harbors a single C-to-U substitution at nt 2576, located at the 3′ end of the internal bulge of ε. DL harbors a 7-nt deletion at the apical loop (nt 2587 to 2593) of ε, and SUS/DL has an additional, 9-nt deletion from the upper portion of the upper stem (nt 2583 to 2586 and nt 2594 to 2598). All ε RNAs were synthesized by using an in vitro transcription kit (Megascript; Ambion) and purified as previously described (20, 24). Baker's yeast tRNA (mix), $tRNA^{lys}$ from *Escherichia coli*, and poly(A) RNA were purchased from Sigma.

In vitro protein priming. The protein priming assay was carried out as previously described (20, 24, 33, 55) with minor modifications. Briefly, the following components were added to a 10-μl reaction mixture: GST-MiniRT2 (ca. 0.1 μM) or 5 μl of the filtered RRL translation reaction mixture expressing the full-length DHBV RT or MiniRT2, ε RNA (or other RNA templates as indicated) (1 μM), 1× proteinase inhibitor cocktail (Roche), 0.5 μl of [α-^{32}P]dGTP (3,000 Ci/mmol and 10 mCi/ml) or another labeled dNTP as indicated, and TMnNK (10 mM Tris-HCl, pH 8.0, 1 mM $MnCl_2$, 15 mM NaCl, 20 mM KCl) or TMgNK (same as TMnNK, except containing 2 mM $MgCl_2$ instead of 1 mM $MnCl_2$) buffer. NP-40 (0.2%, vol/vol) was added to stimulate protein priming by GST-MiniRT2 as previously described (55). For the *trans*-complementation priming assay, purified GST-TP (ca. 0.1 μM) and GST-RT (ca. 0.1 μM) were added to the priming reaction mixture instead of the mini or full-length proteins. For the initiation reaction (I), only a single labeled dNTP was used, whereas for the DNA polymerization reaction (P), the other three dNTPs (i.e., other than the labeled dNTP), which were unlabeled (10 μM each), were also included. The protein priming reaction was then conducted at 30°C for 2 h. The reaction products were resolved by sodium dodecyl sulfate-polyacrylamide gel electrophoresis (SDS-PAGE) and quantified by phosphorimaging.

Limited proteolysis. To a 15-μl proteolysis reaction mixture, 9.5 μl of the protein priming reaction mixture containing the ^{32}P-labeled MiniRT2 was added, together with 0.5 μl of 10× TMnNK or TMgNK buffer and 5 μl (at the indicated

amounts) of the endoproteinase Glu-C (V8 proteinase; Roche). The mixture was then incubated at 25°C for the indicated amounts of time. ^{35}S-labeled luciferase was treated under the same conditions and served as a digestion control. The desalted RRL containing translated luciferase (4 μl) was digested with 5 μl (10 μg) V8 in a total volume of 10 μl at 25°C for 20 min in the presence of either 1× TMnNK or 1× TMgNK. Proteolysis was stopped by adding SDS-PAGE sample buffer and boiling for 5 min. Digestion products were subjected to SDS-PAGE and visualized by autoradiography.

RESULTS

Stimulation of the initiation stage of protein priming by Mn^{2+} compared to that by Mg^{2+}. Although protein priming is a unique function of the hepadnavirus RT that is essential for viral replication, little is known regarding the biochemical properties of this reaction, partly due to its dependence on host chaperone factors (22, 24). The identification of a truncated DHBV RT, the so-called MiniRT2 protein, which can carry out protein priming independent of host chaperone assistance (55), now permits detailed biochemical characterization of protein priming under simple, chemically defined conditions. As divalent metal ions are known to be essential for, and significantly influence, polymerase activity (3, 12, 29, 35, 38, 50), the potential effects of different metal ions on MiniRT2 priming activity were examined. Manganese, iron, cobalt, calcium, zinc, and cadmium were tested at various concentrations ranging from 0.01 to 10 mM for their effects on protein priming by a purified GST fusion protein, GST-MiniRT2, in comparison with magnesium, which has been used as the standard metal ion in the priming reaction (20, 26, 52). First, the covalent attachment of ^{32}P-labeled dGMP to GST-MiniRT2, i.e., the initiation stage of protein priming, was measured. Under the assay conditions, Co^{2+}, Ca^{2+}, Cd^{2+}, and Zn^{2+} were unable to support protein priming (data not shown). Iron acted as a weak cofactor at its optimal concentration of 0.05 mM, which was approximately 50-fold less effective in supporting protein priming than magnesium at its optimal concentration of 2 mM (24) (data not shown). On the other hand, Mn^{2+}, at its optimal concentration of 1 mM, dramatically stimulated the protein priming activity of GST-MiniRT2, being 5- to 10-fold more effective than Mg^{2+} (Fig. 1A, lane 4 versus lane 12).

To test if this effect of Mn^{2+} versus that of Mg^{2+} on protein priming was related to the GST fusion partner in GST-MiniRT2, nonfused MiniRT2, expressed by in vitro translation in RRL, was also tested for protein priming activity with either Mn^{2+} or Mg^{2+}. Furthermore, another truncated DHBV RT, MiniRT2/BstE, which harbors an additional, 14-residue deletion from the C terminus (completely missing the putative thumb subdomain [see Fig. 6]), as well as the full-length RT was also expressed similarly in RRL and tested for protein priming. The DHBV ε RNA was added during the in vitro translation reactions to allow its binding to the translated RT proteins during and immediately after translation (24, 52, 53). Due to the presence of endogenous Mg^{2+} in the RRL in vitro translation system, the translation reaction mixtures containing the RT-ε RNP complex were desalted to remove low-molecular-weight materials by passing through a Sephadex G-50 spin column. The protein priming reaction was then conducted using the desalted translation reaction mixtures in the presence of either Mn^{2+} or Mg^{2+}. In some reactions (Fig. 1C), the purified GST-MiniRT2 was also mixed into the desalted RRL and tested for protein priming, together with the translated RT proteins, in order to test the possible effect of RRL on protein priming with either Mn^{2+} or Mg^{2+}. Control experiments verified that the desalting step efficiently removed the endogenous metal ions such that no priming activity was detectable with the desalted translation reaction mixtures unless Mg^{2+} or Mn^{2+} was added back (data not shown). As shown in Fig. 1B and C, the protein priming activities of MiniRT2, MiniRT2/BstE, and the full-length RT were significantly higher when tested in the presence of Mn^{2+} than when tested in that of Mg^{2+}. This was also true for the purified GST-MiniRT2 protein when it was mixed with RRL. Since MiniRT2/BstE does not contain any thumb subdomain sequence (see Fig. 6A), the residual thumb subdomain in MiniRT2 was apparently not involved in this and other (see below) effects of Mn^{2+} on protein priming.

To summarize, Mn^{2+}, in comparison to Mg^{2+}, was able to significantly stimulate the protein priming activities of all three different DHBV RT proteins tested, both as purified protein and in the RRL translation mix. In addition, since the RT-ε RNP complex was formed in RRL in the presence of Mg^{2+} (approximately 1 mM; Promega) when the RT proteins were expressed by in vitro translation, these results indicated that Mn^{2+} could exert its stimulatory effect on protein priming following RNP formation by affecting the catalytic function itself of the RT proteins.

DNA polymerization by MiniRT2 in the presence of Mn^{2+}. In addition to its stimulatory effect on the initiation stage of protein priming as described above, a more dramatic effect of Mn^{2+} on protein priming was its ability to allow MiniRT2 to transition to the DNA polymerization stage (P). As we reported before (54), the severely truncated MiniRT2 protein was unable, in the presence of Mg^{2+}, to carry out DNA polymerization, i.e., the elongation of the single dGMP residue attached to the RT to form the 4-nt d(GTAA) DNA oligomer (Fig. 1A, lanes 16 and 24; B, lane 1; and E). In contrast, both the purified GST-MiniRT2 protein (Fig. 1A) and the nontagged MiniRT2 and MiniRT2/BstE proteins translated in RRL (Fig. 1B and D) were able to carry out DNA polymerization, as evidenced by an upshift of the labeled RT protein band resulting from the additional mass of the two or three additional nucleotides. This was further confirmed by digesting the initiation and polymerization products with DNase I, which had no effect on initiation (as expected) but shifted the polymerization product down to the same position as the initiation product (Fig. 1D). The much lower incorporation of dCTP than those of the other three dNTPs (Fig. 1A, lanes 5 to 8) suggested that the DNA oligomer synthesized had the same d(GTAA) sequence as that synthesized by the full-length RT in the presence of Mg^{2+} (52, 54). The very small shift (ca. 1 kDa) was also consistent with the very limited extent (i.e., two or three additional nucleotides) of DNA polymerization. On the other hand, DNA polymerization in the presence of Mn^{2+} was complete in that all initiation products were efficiently shifted to the polymerization products (Fig. 1A, B, and D; also see Fig. 2A, 3, and 5), suggesting that all MiniRT2 proteins that initiated protein priming were also able to carry out polymerization. This rather dramatic effect of Mn^{2+}, allowing DNA polymerization by MiniRT2, demonstrated that MiniRT2 actually contained all the necessary sequences required for

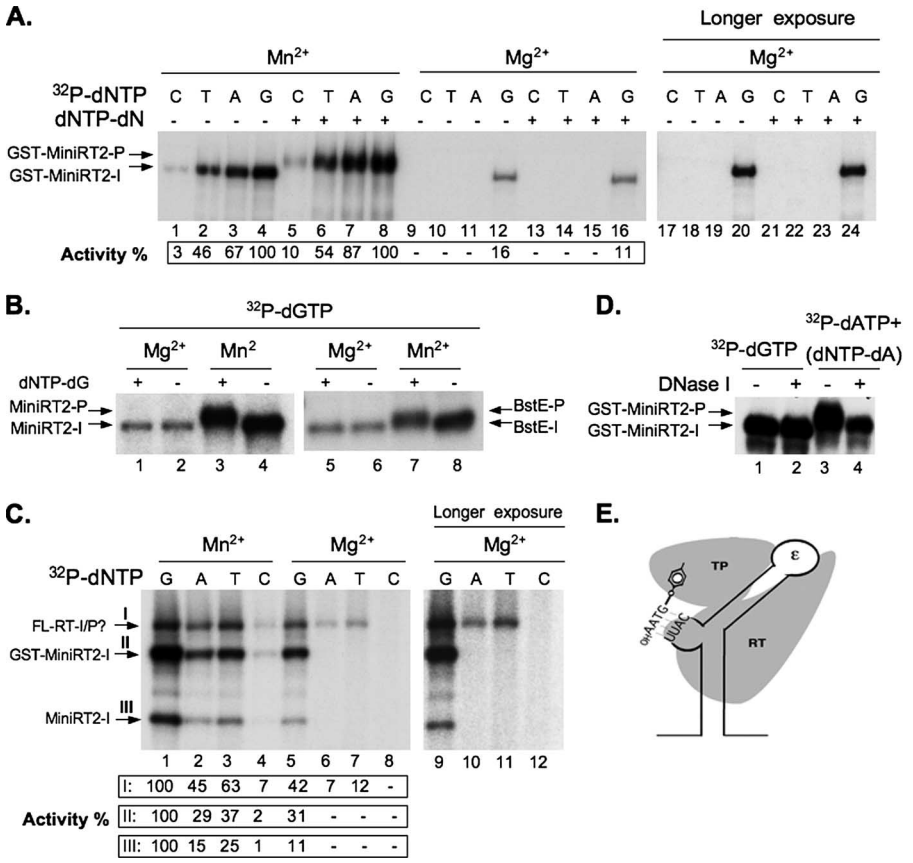

FIG. 1. Effects of Mn^{2+} on DHBV RT initiation and polymerization activity and nucleotide selectivity. (A) Effects of Mn^{2+} and Mg^{2+} on GST-MiniRT2 priming activity. GST-MiniRT2 was tested for protein priming with either the TMnNK buffer (Mn^{2+}; lanes 1 to 8) or the TMgNK buffer (Mg^{2+}; lanes 9 to 16). The indicated [α-^{32}P]dNTP alone was added to the initiation reactions (lanes 1 to 4 and 9 to 12), whereas for the polymerization (P) reaction, both a labeled dNTP and the other three unlabeled dNTPs (dNTP-dN) were added (lanes 5 to 8 and 13 to 16). The reaction products were resolved by SDS-PAGE and detected by autoradiography. Lanes 17 to 24 are lanes 9 to 16, respectively, after longer exposure. Protein priming activity is indicated at the bottom as percentage of activity in the presence of Mn^{2+} and labeled dGTP (lanes 4 and 8 for the initiation and polymerization reactions, respectively). (B) MiniRT2 (lanes 1 to 4) or MiniRT2/BstE (lanes 5 to 8) was translated in RRL, and the desalted translation reaction was then used in the protein priming assay with either Mn^{2+} (lanes 3, 4, 7, and 8) or Mg^{2+} (lanes 1, 2, 5, and 6). In the initiation reactions (lanes 2, 4, 6, and 8), only [^{32}P]dGTP was used, whereas in the polymerization reactions (lanes 1, 3, 5, and 7), the other three (unlabeled) dNTPs (dNTP-dG) were also added. (C) The full-length DHBV RT (FL-RT) and MiniRT2 were translated in RRL, and the desalted translations (2 μl each), together with the purified GST-MiniRT2 protein (ca. 0.1 μM), which was mixed into the desalted translation reaction mixtures, were tested for protein priming (initiation) activity in the same reaction, using only the indicated ^{32}P-labeled nucleotide without any unlabeled dNTPs. Either Mn^{2+} (lanes 1 to 4) or Mg^{2+} (lanes 5 to 8) was used. Lanes 9 to 12 represent lanes 5 to 8, respectively, after longer exposure. Protein priming activity is indicated at the bottom as percentage of activity in the presence of Mn^{2+} and labeled dGTP (lane 1). Roman numerals I, II, and III indicate the primed FL-RT, GST-MiniRT2, and MiniRT2, respectively. (D) DNase sensitivity of the polymerization, but not the initiation, product by GST-MiniRT2. GST-MiniRT2 protein priming was performed in the presence of [α-^{32}P]dGTP (lanes 1 and 2) or [α-^{32}P]dATP plus dNTP-dA (lanes 3 and 4) with the TMnNK buffer. The reaction products were then treated with 1 μg of DNase I at 37°C for 30 min (lanes 2 and 4) or left untreated (lanes 1 and 3) before being resolved by SDS-PAGE. (E) A schematic diagram of the protein priming reaction. Depicted are a computer-predicted DHBV ε RNA structure (28, 36) with its internal bulge sequence (UUAC) as well as the apical loop (the upper and lower stems), the TP and RT domains of the RT protein, and the 4-nt-long DNA oligomer GTAA, covalently attached to TP via the primer tyrosine residue. The initiation reaction refers to the initial attachment of dGMP to TP, whereas the polymerization reaction refers to the subsequent addition of the three further nucleotides following initiation. The initiation (GST-MiniRT2-I, MiniRT2-I, BstE-I, and FL-RT-I) and polymerization (GST-MiniRT2-P, MiniRT2-P, and BstE-P) products from the various RT proteins are indicated. The question mark in panel C (FL-RT-I/P?) indicates that the full-length RT might be able to use the residual amounts of endogenous dNTPs in the desalted RRL to carry out polymerization in the absence of added unlabeled nucleotides.

DNA polymerization but was able to make the transition from initiation to polymerization only in the presence of Mn^{2+}, not in that of Mg^{2+}.

Alteration of nucleotide selectivity during protein priming by Mn^{2+}. Since a well-known effect of Mn^{2+} is that it decreases the fidelity of DNA or RNA synthesis (3, 35), we were interested in determining whether Mn^{2+} would affect the nucleotide selectivity during protein priming. As reported previously (54), MiniRT2 initiated protein priming by using dGTP, but not any other dNTPs (Fig. 1A and C), opposite the template residue C in the internal bulge of the ε RNA (Fig. 1E) when tested in the presence of Mg^{2+}. The low-level initiation activities by dATP and TTP in the case of the full-length RT (Fig. 1C) suggested that the full-length RT may be able to initiate

protein priming by using nucleotides other than dGTP, as also noted earlier (52). Alternatively, the apparent "initiation" activity in the presence of dATP and TTP might actually represent DNA polymerization (see above) due to the presence of residual amounts of endogenous dNTPs present even in the desalted RRL. We noticed that the endogenous dNTPs in RRL were able to support polymerization in the absence of exogenously added dNTPs. The levels of endogenous nucleotides in RRL were substantially decreased by the desalting procedure, as verified by a marked decrease in its ability to support polymerization without exogenous dNTPs. Furthermore, direct measurements using labeled nucleotides confirmed that 97 to 99% of dNTPs were removed by the desalting procedure (data not shown), consistent with the claim made by the supplier (Roche) that the desalting column can remove over 95% of nucleotides in one pass. However, the trace amounts of endogenous dNTPs still remaining in the desalted RRL could potentially support limited polymerization. The DNA polymerization product during protein priming would have the sequence 5′-GTAA-3′ (Fig. 1E), thus explaining the incorporation of labeled dATP and TTP but not dCTP (Fig. 1C). On the other hand, MiniRT2 and GST-MiniRT2 were unable to carry out DNA polymerization in the presence of Mg^{2+} (54), explaining the complete lack of incorporation of any labeled dNTPs other than dGTP (i.e., specific initiation only).

In sharp contrast, the presence of Mn^{2+} allowed incorporation of all four labeled dNTPs during the initiation reaction by GST-MiniRT2, MiniRT2, or full-length RT (Fig. 1A, lanes 1 to 4, and C, lanes 1 to 4). All the RT proteins still preferred dGTP for initiation, which was followed by dATP and TTP, with dCTP being the least active in supporting initiation even in the presence of Mn^{2+}. These results indicated that Mn^{2+} indeed lowered the nucleotide selectivity of the RT proteins during the initiation of protein priming, but some specificity was still retained.

Effect of Mn^{2+} on RNA template specificity during protein priming. It has been well established that DHBV RT strictly uses the internal bulge of the ε RNA as the specific template during protein priming when Mg^{2+} is used as the divalent metal ion (36, 52–54). Given the multiple effects of Mn^{2+} on RT priming activity, as described above, we were interested in determining if the template specificity of protein priming might also be affected by Mn^{2+}. As shown in Fig. 2A, GST-MiniRT2 was indeed able, in the presence of Mn^{2+}, to use RNA templates other than the authentic ε RNA for both initiation and polymerization, albeit at a lower efficiency. These alternative RNA templates included two mutant DHBV ε RNAs, with deletions of the apical loop (DL and SUS/DL) and upper stem (SUS/DL) sequences, and tRNA (either as a mixture of various species [Fig. 2A] or as purified $tRNA^{lys}$ [data not shown]). As expected, none of these heterologous or mutant RNAs were able to support protein priming in the presence of Mg^{2+} (Fig. 2B). On the other hand, some template specificity for protein priming, perhaps for some secondary RNA structural element(s), seemed to be retained since neither the RNA homopolymer poly(A) nor several DNA templates tested were able to support priming even in the presence of Mn^{2+} (Fig. 2C, lane 7, and data not shown). To further test the template, as well as the nucleotide, specificity of protein priming in the

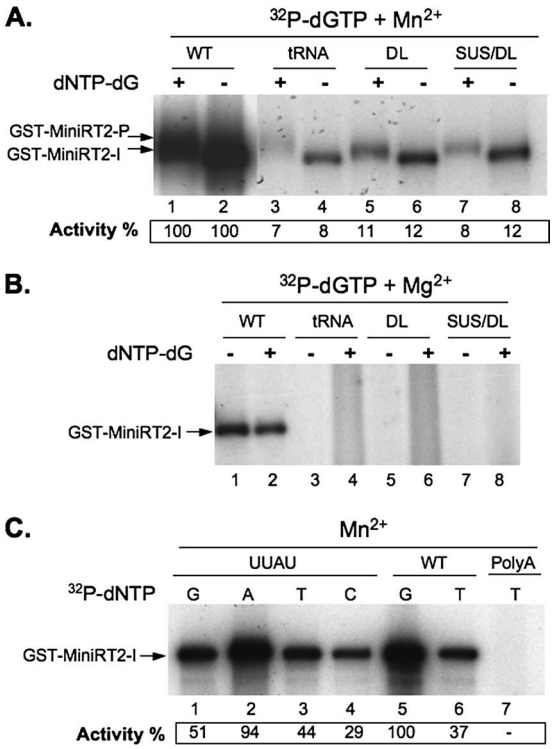

FIG. 2. Effects of Mn^{2+} and Mg^{2+} on template specificity during protein priming. Protein priming activity of GST-MiniRT2 was measured with either Mn^{2+} (A, C) or Mg^{2+} (B). For the initiation reactions (A, lanes 2, 4, 6, and 8, and B, lanes 1, 3, 5, and 7), only [^{32}P]dGTP was included, whereas for the polymerization reactions (A, lanes 1, 3, 5, and 7, and B, lanes 2, 4, 6, and 8), the other three unlabeled dNTPs were also added. The indicated ^{32}P-labeled nucleotide was used alone (without the other unlabeled dNTPs) for panel C. The RNA templates tested include the wild-type DHBV ε RNA (WT); tRNA; three mutant DHBV ε RNAs, with a deletion of the apical loop (DL), a deletion of the apical loop plus sequences of the upper stem (SUS/DL), or a single-nucleotide substitution (C-to-U) at the internal bulge (UUAU); and poly(A) RNA. Protein priming activity is indicated at the bottom as percentage of activity in the presence of the wild-type ε RNA and labeled dGTP (lanes 1 and 2 in panel A and lane 5 in panel C). The initiation (GST-MiniRT2-I) and polymerization (GST-MiniRT2-P) products are indicated.

presence of Mn^{2+}, we used a mutant ε RNA with a single-base (C-to-U) change at the 3′ end of the ε internal bulge (such that the template sequence was changed from UUAC to UUAU). This mutant ε RNA is fully functional in supporting protein priming but, as expected, changes the initiating nucleotide from dGTP to dATP when tested in the presence of Mg^{2+} (54). In the presence of Mn^{2+}, the preferred initiating nucleotide was also changed from dGTP to dATP (Fig. 2C), indicating that GST-MiniRT2 still preferred to initiate protein priming from the authentic position of its cognate RNA template even with Mn^{2+}.

Protein priming in the presence of both Mn^{2+} and Mg^{2+}. The protein priming assays described above were all performed in the presence of either Mn^{2+} or Mg^{2+} alone. To gain further insights into the mechanism of the metal ion effect on protein priming, we measured the protein priming activities in the presence of both ions. In the presence of a constant concentration (2 mM) of Mg^{2+}, the initiation and polymerization

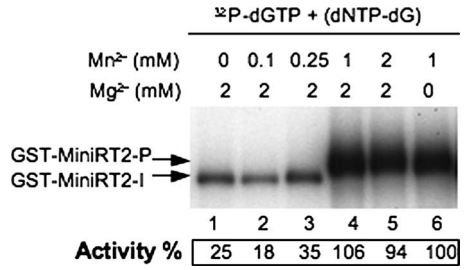

FIG. 3. GST-MiniRT2 protein priming activity in the presence of both Mn^{2+} and Mg^{2+}. GST-MiniRT2 was tested for protein priming activity in the presence of [^{32}P]dGTP, dNTP-dG, and the indicated concentrations of Mn^{2+} and Mg^{2+}. Protein priming activity is indicated at the bottom as percentage of priming activity in 1 mM Mn^{2+} alone (lane 6). The initiation (GST-MiniRT2-I) and polymerization (GST-MiniRT2-P) products are indicated.

activities of GST-MiniRT2 were tested in the presence of increasing concentrations of Mn^{2+}. As depicted in Fig. 3, the protein priming profile was changed from the typical Mg^{2+}-dependent reaction (weak initiation and no polymerization) to the typical Mn^{2+}-dependent reaction (strong initiation and polymerization) when the Mn^{2+} concentration reached 1 mM, i.e., half of the Mg^{2+} concentration. The change in the activity profile, in terms of both the increase in initiation and the ability to transition to polymerization, occurred within an narrow range of Mn^{2+} concentration (from 0.25 to 1 mM), with no evidence for an intermediate stage (e.g., weak initiation yet with polymerization), suggesting that the stimulation of initiation and the facilitation of polymerization by Mn^{2+} were mechanistically linked, probably through the induction of an alternative RT conformation that had much higher initiation activity and also was able to carry out polymerization following initiation (see below).

Effect on the sensitivity of protein priming to PFA inhibition. It is well known that most nucleoside analogs and the pyrophosphate analog PFA are able to inhibit hepadnavirus DNA synthesis following protein priming but are ineffective in inhibiting protein priming itself (44, 52), presumably because the RT protein adopts a conformation (priming mode) during protein priming that is distinct from that involved in subsequent DNA synthesis. Given the presumed effect of Mn^{2+} on RT structure during protein priming, it was of interest to determine whether protein priming in the presence of Mn^{2+} would display a sensitivity profile different from that in the presence of Mg^{2+}. We first tested the sensitivity of purified GST-MiniRT2 toward PFA inhibition in either the initiation or the polymerization reaction. The initiation reaction was found to be completely refractory to PFA inhibition (up to a concentration of 1 mM) in the presence of Mg^{2+} and was inhibited only slightly in the presence of Mn^{2+} (reduced to ca. 70% by 1 mM PFA) (Fig. 4A). In contrast, polymerization was rather sensitive to PFA inhibition in a dose-dependent fashion, with a 50% inhibitory concentration of around 5 to 10 μM (Fig. 4B).

We then tested the nonfused MiniRT2 and the full-length RT expressed in RRL for their sensitivities to PFA. Again, the initiation reaction carried out by these proteins, like that by the purified GST-MiniRT2, was completely refractory to PFA inhibition with Mg^{2+} or only slightly inhibited with Mn^{2+} (data not shown). On the other hand, the polymerization reaction was again sensitive to PFA when Mn^{2+} was used (Fig. 4C). The inhibitory effects of PFA on MiniRT2 and the full-length RT were not as strong as that on the purified GST-MiniRT2 protein, with a 50% inhibitory concentration approaching 100 μM. However, the purified GST-MiniRT2 protein was also similarly less sensitive to PFA when tested with RRL (Fig. 4C), suggesting that all three RT proteins could be inhibited to similar degrees by PFA, but RRL appeared to decrease the effectiveness of PFA in inhibiting polymerization, possibly due to the binding of PFA to proteins in RRL, which would decrease the

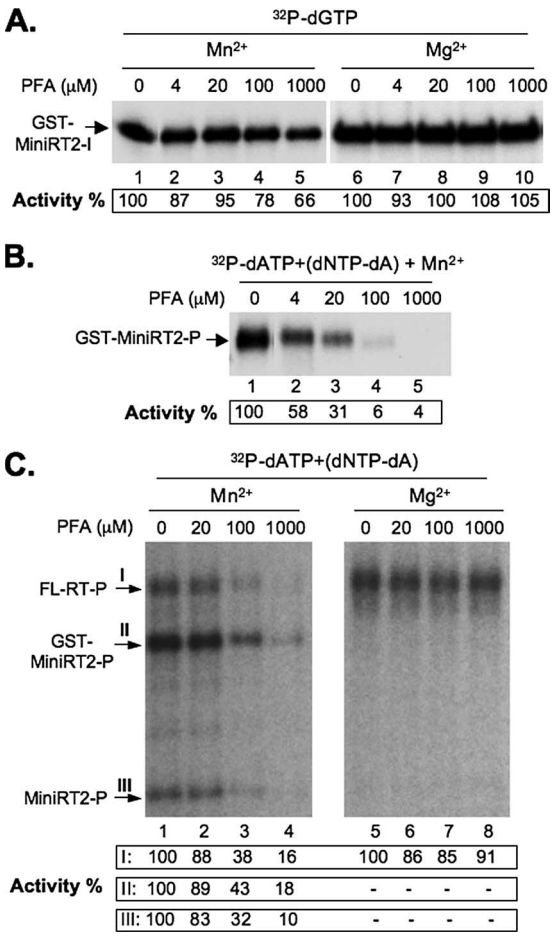

FIG. 4. Effects of Mn^{2+} versus those of Mg^{2+} on PFA inhibition of protein priming. Purified GST-MiniRT2 (A, B) or in vitro-translated full-length DHBV RT (FL-RT) and MiniRT2 (in desalted RRL), together with GST-MiniRT2 mixed into RRL after translation and desalting (C) (as described for Fig. 1C), were tested for initiation with only [^{32}P]dGTP (A) or for polymerization with [^{32}P]dATP plus unlabeled dNTP-dA (B, C). The priming reactions were carried out in the presence of either Mn^{2+} (A, lanes 1 to 5; B; and C, lanes 1 to 4) or Mg^{2+} (A, lanes 6 to 10, and C, lanes 5 to 8). The pyrophosphate analog PFA was added at the indicated concentrations. Protein priming activity is indicated at the bottom as percentage of activity without PFA under each condition. The initiation (GST-MiniRT2-I) and polymerization (GST-MiniRT2-P, FL-RT-P, and MiniRT2-P) products are indicated. Roman numerals I, II, and III in panel C indicate the polymerization products from FL-RT, GST-MiniRT2, and MiniRT2, respectively.

effective PFA concentration in RRL. In contrast, polymerization carried out by the full-length RT in the presence of Mg^{2+} was resistant to PFA up to 1 mM (Fig. 4C), as reported before (52). As MiniRT2 or GST-MiniRT2 was unable to carry out polymerization in the presence of Mg^{2+}, it was not possible to test the effect of PFA on polymerization by these truncated proteins in the presence of Mg^{2+}. In any case, the differential sensitivity of the initiation reaction versus that of the polymerization reaction to PFA inhibition indicated that the RT proteins likely underwent a conformational transition as they progressed from the initiation to the polymerization stage of protein priming and consequently acquired PFA sensitivity. On the other hand, the sensitivity of polymerization to PFA inhibition in the presence of Mn^{2+}, but not Mg^{2+}, suggested that the RT conformation during polymerization might also be different depending on the different ions.

Metal ion effects on protein priming in the *trans*-complementation assay. It has been reported that separate TP and RT domains, as isolated polypeptides, can complement each other to reconstitute protein priming, whereby the RT domain is able to synthesize a short DNA oligomer by using the separated TP domain as the primer (9, 30). We were interested in determining if Mn^{2+} and Mg^{2+} would also have differential effects in this *trans*-complementation priming assay. The TP and RT domains, containing the same respective domain sequences as those present in MiniRT2, were expressed and purified as separate GST fusion proteins (GST-TP and GST-RT, respectively). They were then mixed together with the ε RNA and tested for protein priming in the presence of either Mn^{2+} or Mg^{2+}. Again, Mn^{2+} was able to dramatically stimulate the initiation stage of protein priming in this assay, up to 30-fold more effective than Mg^{2+} (Fig. 5A). Furthermore, the truncated RT domain was able to carry out DNA polymerization in the presence of Mn^{2+}, but not Mg^{2+}, as described above in the case of MiniRT2. In addition, the nucleotide selectivities in this *trans*-complementation priming assay were similarly reduced by Mn^{2+}. Thus, all four dNTPs were able to initiate protein priming (although dGTP was still preferred) in the presence of Mn^{2+} whereas only dGTP was able to do so in the presence of Mg^{2+} (Fig. 5B). Therefore, Mn^{2+} and Mg^{2+} showed similar differential effects on the initiation and polymerization activities as well as the nucleotide selectivity in the *trans*-complementation priming activity, as they did in the single-protein assay.

Partial proteolysis revealed RT structural differences in the presence of Mn^{2+} versus that of Mg^{2+} and during initiation versus polymerization. The above-mentioned results, taken together, strongly suggested that Mn^{2+} and Mg^{2+} induced structural differences in the RT proteins, as reflected in their effects on RT functions (initiation, polymerization, nucleotide selectivity, and template specificity) and inhibitor (PFA) sensitivity. Currently, very little is known about the structural details of hepadnavirus RT proteins, due to the lack of any high-resolution structural data. On the other hand, limited proteolysis, which leads to more-frequent cleavages at surface-accessible sites than at less accessible sites, has been used with some success to reveal the RT conformational maturation as induced by cellular chaperones (43) and ε binding (47, 48). We therefore decided to adopt this approach in an attempt to directly demonstrate any RT structural differences induced by Mn^{2+} versus Mg^{2+} as well as the presumed RT structural transition from initiation to polymerization. To optimize the proteolysis conditions, pilot experiments were conducted using several different RT proteins (the full-length RT, GST-MiniRT2, and MiniRT2) and various proteinases (V8, papain, and trypsin). Based on the following preliminary observations, we chose to use V8 digestion of the primed ([^{32}P]dGMP-labeled) MiniRT2 protein (no GST fusion) throughout this study. First, digestion of a control protein (luciferase) by use of V8 showed that partial V8 proteolysis was unaffected by either Mn^{2+} or Mg^{2+} (Fig. 6B), as expected from the metal ion independence of V8 protease (15, 19). This was important since we were interested in comparing the RT digestion pattern in Mn^{2+} with that in Mg^{2+}. Second, since only enzymatically active RT proteins could be labeled by ^{32}P incorporation, focusing on the labeled proteolytic fragments allowed us to examine the digestion patterns of exclusively active proteins without interference from extraneous digestion products derived from inactive RT proteins. Third, since the only ^{32}P-labeled residue was Y96 and there were no V8 cleavage sites N-terminal to Y96 in MiniRT2, all labeled partial proteolysis species must have been derived from cleavage C-terminal to Y96 (Fig. 6A), making the identification of the digestion products relatively straightforward. In contrast, the multiple V8 cleavage sites present N-terminal to Y96 in the full-length RT and GST-MiniRT2 made the assignment of the digestion products rather problematic. Indeed, as shown in Fig. 6C, distinct fragmentation patterns of ^{32}P-labeled MiniRT2 were readily detectable by SDS-PAGE and autoradiography following limited V8 digestion.

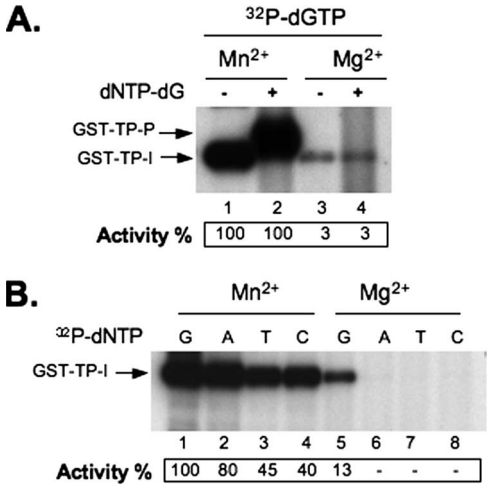

FIG. 5. Effects of Mn^{2+} and Mg^{2+} on protein priming in the *trans*-complementation assay using separate TP and RT domains. Purified GST-TP and GST-RT domains were mixed together for the *trans*-complementation priming assay, with either [^{32}P]dGTP alone (for initiation) (A, lanes 1 and 3) or further supplementation with unlabeled dNTP-dG (for polymerization) (A, lanes 2 and 4). Each different labeled dNTP (as indicated) without the other unlabeled nucleotides was used in the initiation assay whose results are shown in panel B. The priming reactions were performed either with Mn^{2+} (A, lanes 1 and 2, and B, lanes 1 to 4) or with Mg^{2+} (A, lanes 3 and 4, and B, lanes 5 to 8). In panel A, protein priming activity is indicated at the bottom as percentage of priming activity (initiation, lane 1; polymerization, lane 2) with Mn^{2+}. In panel B, priming activity is indicated as percentage of priming activity (initiation) with [^{32}P]dGTP and Mn^{2+} (lane 1).

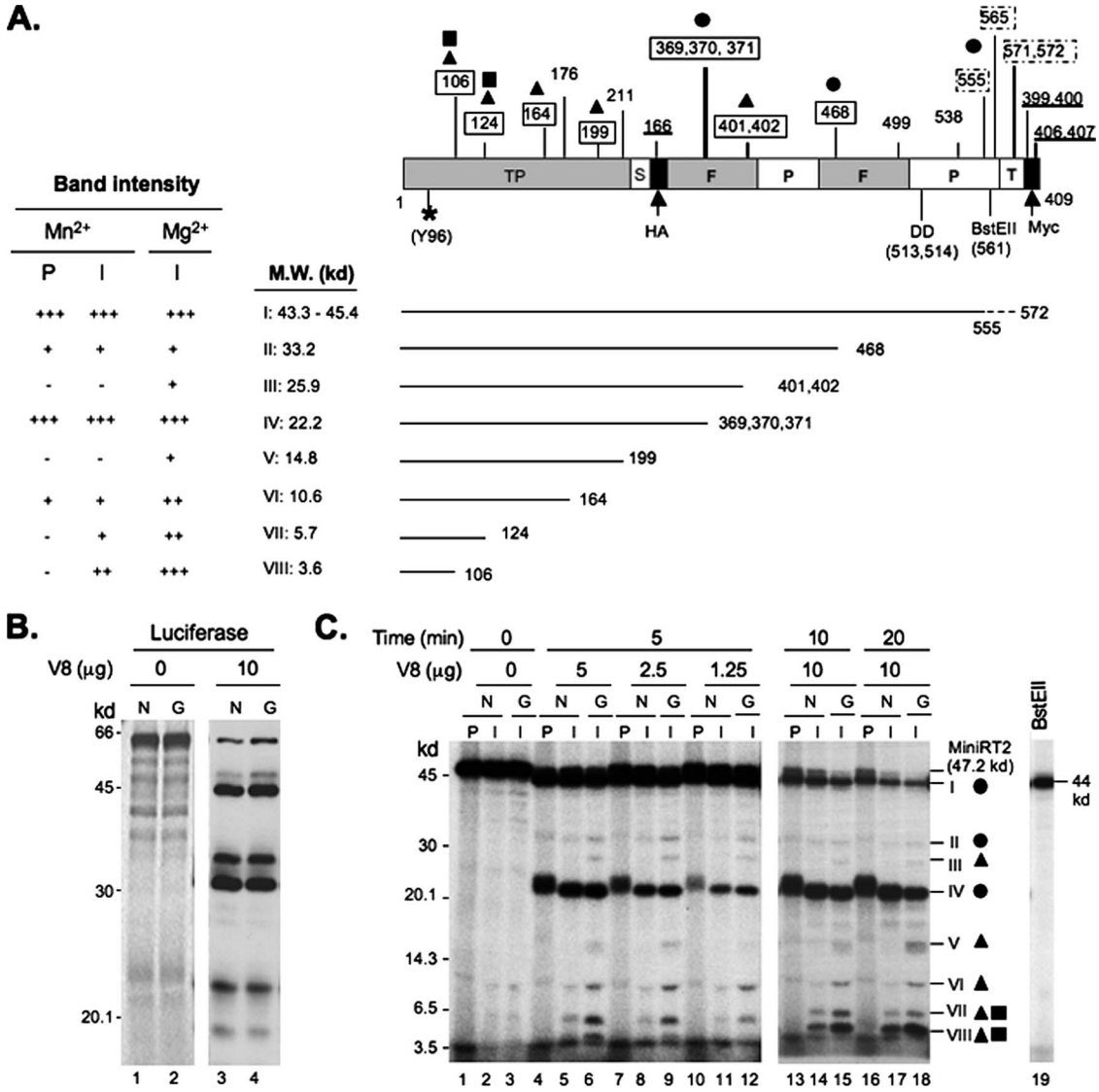

FIG. 6. Partial V8 proteolysis of primed MiniRT2. (A) Schematic diagram of MiniRT2 domain structure and summary of digestion results. MiniRT2 is denoted as a box on the top with its domain and subdomain designation. S, spacer (shortened); F, finger subdomain; P, palm subdomain; T, thumb subdomain (residual); HA, hemagglutinin epitope; Myc, Myc epitope. The numbers below the box refer to the positions in MiniRT2 (1 to 409), except that those in parenthesis denote the actual positions in the full-length RT (the primer Y96, attached to [^{32}P]dGTP, which is symbolized by *; D513/D514, within the catalytic YMDD motif; and the BstE II restriction site at position 561). Position 2 in MiniRT2 corresponds to position 75 in the full-length RT. The numbers above the box indicate all predicted V8 cleavage sites (E and DG) (15, 19), with the boxed numbers indicating observed cleavage sites. Dashed boxes denote the uncertainty in accurately assigning the closely clustered cleavage sites at positions 555, 565, and 571/572. All numbers on the top refer to the positions in the full-length RT, except that the underlined numbers, which indicate predicted V8 sites within the HA and Myc epitope tags, denote the positions in MiniRT2. Circles, triangles, and squares represent the three different classes of partial digestion products as explained for panel C. Summarized below the MiniRT2 domain diagram are the observed V8 partial digestion products, I to VIII, represented by the solid lines ending with their respective cleavage site numbers (referring to the positions in the full-length RT), with their predicted sizes indicated. The dashed line at the end of species I denotes the uncertainty in assigning the closely spaced sites between positions 555 and 572. To the left are summarized the band intensities representing each of the eight species as detected by autoradiography (C). + to +++, increasing in intensity (abundance); −, undetectable. The intensities of species VI, VII, and VIII derived from initiations with Mg^{2+} were approximately threefold stronger than those with Mn^{2+}, as quantified from multiple experiments. (B) Control digestion of ^{35}S-labeled luciferase by V8 in the presence of Mn^{2+} (N; lane 3) or Mg^{2+} (G; lane 4). The digestion products were resolved by SDS-PAGE and detected by autoradiography. Undigested luciferase was used as a control (lanes 1 and 2). The molecular mass (M.W.) standards are indicated to the left. (C) Digestion of primed MiniRT2. Following the initiation reaction (I) with either Mn^{2+} (N) or Mg^{2+} (G) or the polymerization reaction (P) with Mn^{2+} (N), MiniRT2 was digested with increasing amounts of V8 (1.25, 2.5, and 5 μg) at 25°C for 5 min (lanes 4 to 12) or with a fixed amount (10 μg) V8 for 10 or 20 min (lanes 13 to 18). The digestion products were resolved by SDS-PAGE and detected by autoradiography. Undigested MiniRT2 following the initiation (lanes 2 and 3) or polymerization (lane 1) reaction was used as a control. The molecular mass standards are indicated to the left. The primed MiniRT2-BstEII (lane 19) was used as an additional molecular mass standard (44 kDa). The digestion products are indicated on the right by Roman numerals I to VIII as in panel A. Circles denote the proteolysis species (I, II, and IV) that showed similar abundances in all three MiniRT2 samples (initiation with Mn^{2+} or Mg^{2+} or polymerization). Triangles denote the species (III, V, VI, VII, and VIII) that were more abundant in the initiation sample with Mg^{2+} than in that with Mn^{2+}. The squares represent two species (VII and VIII) that were uniquely absent from the polymerization sample. The proteolytic species derived from the polymerization products (I, II, IV,

As depicted in Fig. 6, we were able to obtain partial V8 cleavage in most (but not all) predicted cleavage sites. A total of 8 (I to VIII) cleavage products were readily detected and assigned, following partial V8 digestion using either a protease titration (Fig. 6C, lanes 4 to 12) or a time course (Fig. 6C, lanes 13 to 18) experiment. By comparing the digestion patterns of ^{32}P-labeled MiniRT2 following initiation (MiniRT2-I) with either Mn^{2+} or Mg^{2+} or following polymerization (MiniRT2-P), three different classes of partial digestion products were identifiable. First, the intensities of three species (I, II, and IV) were identical or similar under all three conditions, indicating that the cleavage sites at E555/565/571/572 (clustered at the extreme C terminus, producing species I), D468 (at a DG motif [15, 19] in the putative finger subdomain, producing species II), and E369/370/371 (clustered within the putative finger subdomain, producing species IV) were equally accessible in all three primed MiniRT2 proteins. The strong intensities of species I and IV suggested that the C-terminal end and E369/370/371 were well exposed to proteolysis, whereas the weak intensity of species II suggested that D468 was relatively inaccessible to proteolysis. Nevertheless, the accessibility of these sites was not affected by the metal ions or the transition from initiation to polymerization. Second, two species (III and V) derived from MiniRT2-I with Mg^{2+} were absent from that with Mn^{2+}, and three species (VI, VII, and VIII) derived from MiniRT2-I with Mn^{2+} were less abundant than those with Mg^{2+}, suggesting that the cleavage sites at E401/402 (in the putative finger subdomain, producing species III), E199 (in the TP domain, producing species V), and E164, E124, and E106 (all in the TP domain, producing species VI, VII, and VIII, respectively) were more accessible in the initiated MiniRT2 protein when the initiation reaction was performed with Mg^{2+} than with Mn^{2+}. This was evident in both the concentration titration (lanes 6, 9, and 12 versus lanes 5, 8, and 11, respectively) and the time course (lanes 15 and 18 versus lanes 14 and 17, respectively) experiments. Third, two species, VII and VIII, were uniquely absent from MiniRT2-P (i.e., following DNA polymerization in the presence of Mn^{2+}) (lanes 4, 7, 10, 13, and 16 versus lanes 5, 8, 11, 14, and 17, respectively), suggesting that the cleavage sites at E124 and E106 in the TP domain became less or not accessible to V8 digestion when MiniRT2 transitioned from the stage of initiation to polymerization during protein priming. Although the intensities of some digestion products (species II, III, and V) were fairly weak (due to their relative inaccessibility to proteolysis under the partial digestion conditions), the distinct patterns detected in the presence of the different metal ions or following the transition to polymerization were highly reproducible.

In summary, the partial V8 digestion provided direct evidence indicating that Mn^{2+} and Mg^{2+} indeed induced differential RT folding, as anticipated from their distinct effects on RT activities. The differences in the RT structure were particularly pronounced in the TP domain but also could be detected in the putative finger subdomain of the RT domain. Furthermore, the proteolysis results indicated that the RT protein underwent a conformational change localized in the TP domain, at least when tested in the presence of Mn^{2+}, as it progressed from the initiation to the polymerization stage of protein priming.

DISCUSSION

The hepadnavirus RT protein plays multiple essential roles at the different stages of the viral life cycle, including pgRNA encapsidation, protein-primed initiation of reverse transcription, and subsequent minus and plus strand DNA synthesis. To carry out these multiple functions, RT likely undergoes dynamic changes in its structure, which remains poorly understood at present. In particular, the protein priming reaction, in which the TP and RT domains and the ε RNA must all interact precisely to allow proper DNA synthesis, almost certainly requires an RT conformation (termed the priming mode) (23, 24) that is distinct from that involved in the subsequent, more "generic" DNA elongation reaction. The requirement for host chaperone assistance in the protein priming reaction (specifically, RT-ε RNP formation) (22–24) is but one reflection of such a distinct conformational demand. Also in support of the distinct requirements for protein priming versus those for the subsequent DNA elongation are observations that certain RT mutations, and many nucleoside analogs and the pyrophosphate analog PFA, can block DNA elongation but have no effect on protein priming (41, 44, 52). Furthermore, the recent identification of the DHBV MiniRT2 protein, which is functional in the first step of protein priming, the covalent attachment of the first nucleotide (dGMP) to TP (initiation), but defective in the subsequent addition of three more nucleotides (polymerization) (54), suggests that even the protein priming reaction itself can be further divided into two distinct stages that require different RT structures.

By conducting the protein priming reaction, using the divalent metal ion Mn^{2+} as an alternative to the standard Mg^{2+}, we now provide functional and structural evidence that suggests that initiation and polymerization require distinct RT conformations, as predicted by the two-step priming hypothesis. Most strikingly, in the presence of Mn^{2+}, MiniRT2 was as active in polymerization as it was in initiation even though it is severely defective in polymerization with Mg^{2+}. This effectively ruled out the possibility that MiniRT2 simply lacks some essential sequences required for polymerization. Rather, our results indicate that MiniRT2 (and, by inference, the full-length RT as well) undergoes a conformational change in order to progress from the initiation to the polymerization stage

and VI) were upshifted slightly compared to the corresponding species from the initiation products due to the extra mass (ca. 1 kDa) of the two or three additional nucleotides. Note that the circles, triangles, and squares in panels A and C are used to indicate the same corresponding classes of cleavage site accessibility or species abundance. Also, since the priming activity of MiniRT2 in the presence of Mn^{2+} was stronger than that in the presence of Mg^{2+}, the amounts of samples loaded to the gel were normalized to display the same amount of labeled MiniRT2 under each condition, but the amounts of samples (RRL containing primed MiniRT2) used in the V8 digestion reactions were the same under all three conditions.

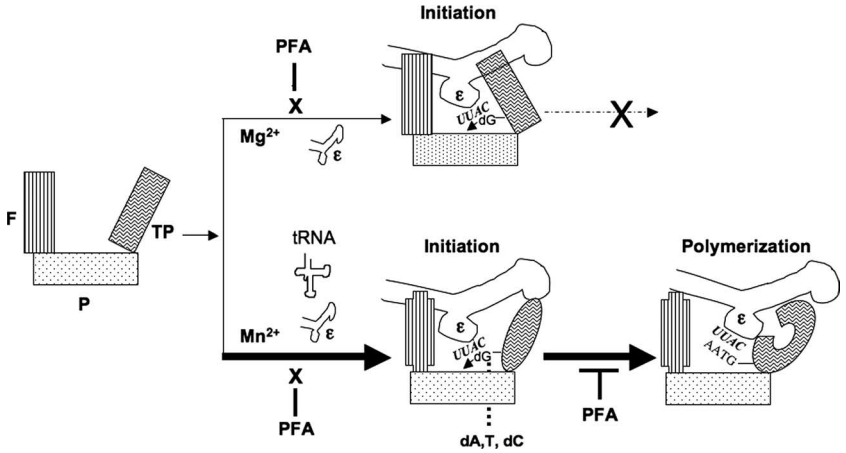

FIG. 7. Model of Mn^{2+} versus Mg^{2+} effects on protein priming of MiniRT2. The domains and subdomains of the RT are depicted as blocks. F and P represent the "finger" and "palm" subdomains of the RT domain, respectively. The residual thumb subdomain in MiniRT2 is omitted for clarity, as it is not involved in the metal ion effects reported here. The ε RNA is depicted as a stem-loop structure, with its internal bulge (the template for protein priming) facing the palm subdomain. The tRNA is depicted as a cloverleaf. MiniRT2 and likely the full-length RT (not depicted; see text for details) adopt two distinct conformations depending on the presence of Mn^{2+} or Mg^{2+}, which affect its efficiency in the initiation of protein priming (with the one in Mn^{2+} having much higher activity, as denoted by the thick arrowhead), competence in polymerization (only with Mn^{2+}), template and nucleotide specificity (relaxed with Mn^{2+}), and sensitivity to PFA inhibition (polymerization being sensitive to PFA in Mn^{2+} but not Mg^{2+}). The changes in the TP and F subdomain block shapes denote the structural differences revealed by V8 digestion in MiniRT2 in the presence of Mn^{2+} versus that observed with Mg^{2+} and during the transition from initiation to polymerization. See text for details.

during protein priming. It appears that this structural transition, for MiniRT2, could occur only in the presence of Mn^{2+}, not in that of Mg^{2+} (Fig. 7). The limited V8 proteolysis experiment provided direct, albeit low-resolution, structural evidence for this conformational transition, particularly in the structurally unique TP domain. Thus, not only did the partial V8 digestion patterns of MiniRT2 differ following initiation with Mn^{2+} versus that with Mg^{2+}, a structural difference which may also underlie the other metal ion effects on protein priming (see below) in addition to polymerization, but two cleavage sites near the primer Y96 within the TP domain specifically became inaccessible following polymerization. Obviously, the full-length RT is able to make the putative conformational transition in the presence of either ion. Further studies to understand what accounts for this interesting difference between the full-length and the truncated RT proteins may provide novel insights into the RT conformational dynamics observed during protein priming.

Besides its dramatic effect on polymerization, Mn^{2+} also showed a number of other interesting effects on protein priming in comparison to Mg^{2+}. As reported for a number of other DNA or RNA polymerases (3, 35, 38), Mn^{2+} increased the efficiency of DNA synthesis by the hepadnavirus RT but decreased the specificity of nucleotide incorporation (fidelity). It also relaxed the template specificity of protein priming such that the RT proteins could carry out protein priming, albeit weakly, with RNA templates other than the authentic ε RNA. It appears that any RNA with some secondary structure (stem loop), but not linear RNA, may weakly support protein priming with Mn^{2+}. These metal ion effects may be partly responsible for some of the discrepancies reported previously regarding the requirements for protein priming in vitro, as different ionic conditions were apparently used in different reports (7, 26, 32, 50), suggesting that caution is needed in comparing results under otherwise seemingly similar conditions. As is true for the other polymerases, the exact structural basis for these functional effects of metal ions on the RT proteins remains to be elucidated. However, the differential V8 partial digestion pattern of MiniRT2 in the presence of Mn^{2+} versus that observed with Mg^{2+} suggests that some structural differences in the TP as well as the RT (specifically the finger subdomain) domain may be at least partially responsible. We note that a recent report also showed that the C-terminal proximal region of TP (around E164) became exposed to V8 digestion upon host chaperone-mediated activation of RT (43). The protease accessibility of this same TP region in MiniRT2, in the absence of host chaperone help, is consistent with the fact that MiniRT2 can fold into an active form independent of host chaperones. On the other hand, the greater accessibility of this region of MiniRT2 in the presence of Mg^{2+} than in that of Mn^{2+}, despite the much lower priming activity in the presence of Mg^{2+}, suggests that the correlation between priming activity and protease accessibility in this region may not be straightforward. The apparent inaccessibility of the more N-terminal region of TP (E106 and E124) found in that study was likely due to the fact that a mixture of Mg^{2+} and Mn^{2+} was used and the RT structure was examined following polymerization, which we have shown here to correlate with V8 inaccessibility in this TP region. However, our results clearly showed that this same region was in fact accessible, transiently, during the initiation stage of protein priming, particularly when Mg^{2+} was used. Additionally, the metal ions may also affect the ε RNA structure, which could, in turn, affect protein priming through its role as both the specific template and the activator of RT function (32, 48, 53). However, the effect of Mn^{2+} persisted even after the RT-ε RNP complex had already formed in the presence of Mg^{2+} (during translation in RRL), indicating that the metal ion effect could occur independent of any potential effect on RT-ε binding. Furthermore, the dramatic activation of RT priming activity by Mn^{2+} may prove useful in obtaining

large amounts of RT proteins with high specific activity for high-resolution structural analysis, an important but still elusive goal in the HBV field.

It was intriguing that the metal ions also affected the sensitivity of protein priming to inhibition by the pyrophosphate analog PFA. It is well known that PFA does not inhibit protein priming (either initiation or polymerization) (in the presence of Mg^{2+}), despite being a potent inhibitor of HBV DNA elongation (23, 52). However, our results showed that the polymerization step of protein priming was subject to inhibition by PFA when Mn^{2+} was present. This was true for both the full-length RT and MiniRT2. On the other hand, PFA did not inhibit the initiation reaction by any RT protein tested with either Mn^{2+} or Mg^{2+}. These results suggest that the RT conformation required for the first stage of protein priming may be fundamentally different from the "generic" elongation conformation that is susceptible to PFA inhibition, but the conformation during the polymerization stage may share some similarities with the postpriming elongation mode. As PFA is thought to bind to the polymerase active site and this binding can also be affected indirectly by changes elsewhere distant from the active site (13, 34, 46), the RT conformational transition from initiation to polymerization that may be responsible for the dramatic increase in PFA sensitivity could occur within the RT and/or TP domain (Fig. 7), as revealed by partial V8 digestion. In any case, the ability to inhibit the polymerization stage of protein priming by a conventional polymerase inhibitor, such as PFA, suggests that it may yet be feasible to target this stage of protein priming for antiviral development. More generally, a better understanding of the structural dynamics observed during protein priming, a unique and essential early step in HBV reverse transcription, should facilitate the design of novel and effective anti-HBV therapy.

ACKNOWLEDGMENTS

We thank Morgan Boyer for excellent technical assistance.

This work was supported by a Public Health Service grant from the National Institutes of Health and a Research Scholar Grant from the American Cancer Society.

REFERENCES

1. **Abraham, T. M., and D. D. Loeb.** 2006. Base pairing between the 5′ half of ε and a *cis*-acting sequence, Φ, makes a contribution to the synthesis of minus-strand DNA for human hepatitis B virus. J. Virol. **80:**4380–4387.
2. **Abraham, T. M., and D. D. Loeb.** 2007. The topology of hepatitis B virus pregenomic RNA promotes its replication. J. Virol. **81:**11577–11584.
3. **Arnold, J. J., S. K. Ghosh, and C. E. Cameron.** 1999. Poliovirus RNA-dependent RNA polymerase (3D(pol)). Divalent cation modulation of primer, template, and nucleotide selection. J. Biol. Chem. **274:**37060–37069.
4. **Bartenschlager, R., M. Junker-Niepmann, and H. Schaller.** 1990. The P gene product of hepatitis B virus is required as a structural component for genomic RNA encapsidation. J. Virol. **64:**5324–5332.
5. **Bartenschlager, R., C. Kuhn, and H. Schaller.** 1992. Expression of the P-protein of the human hepatitis B virus in a vaccinia virus system and detection of the nucleocapsid-associated P-gene product by radiolabelling at newly introduced phosphorylation sites. Nucleic Acids Res. **20:**195–202.
6. **Bartenschlager, R., and H. Schaller.** 1992. Hepadnaviral assembly is initiated by polymerase binding to the encapsidation signal in the viral RNA genome. EMBO J. **11:**3413–3420.
7. **Beck, J., and M. Nassal.** 2003. Efficient Hsp90-independent in vitro activation by Hsc70 and Hsp40 of duck hepatitis B virus reverse transcriptase, an assumed Hsp90 client protein. J. Biol. Chem. **278:**36128–36138.
8. **Beck, J., and M. Nassal.** 1998. Formation of a functional hepatitis B virus replication initiation complex involves a major structural alteration in the RNA template. Mol. Cell. Biol. **18:**6265–6272.
9. **Beck, J., and M. Nassal.** 2001. Reconstitution of a functional duck hepatitis B virus replication initiation complex from separate reverse transcriptase domains expressed in *Escherichia coli*. J. Virol. **75:**7410–7419.
10. **Beck, J., and M. Nassal.** 1997. Sequence- and structure-specific determinants in the interaction between the RNA encapsidation signal and reverse transcriptase of avian hepatitis B viruses. J. Virol. **71:**4971–4980.
11. **Chang, L. J., R. C. Hirsch, D. Ganem, and H. E. Varmus.** 1990. Effects of insertional and point mutations on the functions of the duck hepatitis B virus polymerase. J. Virol. **64:**5553–5558.
12. **Crotty, S., D. Gohara, D. K. Gilligan, S. Karelsky, C. E. Cameron, and R. Andino.** 2003. Manganese-dependent polioviruses caused by mutations within the viral polymerase. J. Virol. **77:**5378–5388.
13. **Crumpacker, C. S.** 1992. Mechanism of action of foscarnet against viral polymerases. Am. J. Med. **92(2A):**3S–7S.
14. **Das, K., X. Xiong, H. Yang, C. E. Westland, C. S. Gibbs, S. G. Sarafianos, and E. Arnold.** 2001. Molecular modeling and biochemical characterization reveal the mechanism of hepatitis B virus polymerase resistance to lamivudine (3TC) and emtricitabine (FTC). J. Virol. **75:**4771–4779.
15. **Drapeau, G. R., Y. Boily, and J. Houmard.** 1972. Purification and properties of an extracellular protease of Staphylococcus aureus. J. Biol. Chem. **247:**6720–6726.
16. **Flodell, S., M. Petersen, F. Girard, J. Zdunek, K. Kidd-Ljunggren, J. Schleucher, and S. Wijmenga.** 2006. Solution structure of the apical stem-loop of the human hepatitis B virus encapsidation signal. Nucleic Acids Res. **34:**4449–4457.
17. **Girard, F. C., O. M. Ottink, K. A. Ampt, M. Tessari, and S. S. Wijmenga.** 2007. Thermodynamics and NMR studies on duck, heron and human HBV encapsidation signals. Nucleic Acids Res. **35:**2800–2811.
18. **Hirsch, R. C., J. E. Lavine, L. J. Chang, H. E. Varmus, and D. Ganem.** 1990. Polymerase gene products of hepatitis B viruses are required for genomic RNA packaging as well as for reverse transcription. Nature **344:**552–555.
19. **Houmard, J., and G. R. Drapeau.** 1972. Staphylococcal protease: a proteolytic enzyme specific for glutamoyl bonds. Proc. Natl. Acad. Sci. USA **69:**3506–3509.
20. **Hu, J., and D. Anselmo.** 2000. In vitro reconstitution of a functional duck hepatitis B virus reverse transcriptase: posttranslational activation by Hsp90. J. Virol. **74:**11447–11455.
21. **Hu, J., D. Flores, D. Toft, X. Wang, and D. Nguyen.** 2004. Requirement of heat shock protein 90 for human hepatitis B virus reverse transcriptase function. J. Virol. **78:**13122–13131.
22. **Hu, J., and L. Lin.** RNA-protein interactions in hepadnavirus reverse transcription. Front. Biosci., in press.
23. **Hu, J., and C. Seeger.** 1996. Expression and characterization of hepadnavirus reverse transcriptases. Methods Enzymol. **275:**195–208.
24. **Hu, J., and C. Seeger.** 1996. Hsp90 is required for the activity of a hepatitis B virus reverse transcriptase. Proc. Natl. Acad. Sci. USA **93:**1060–1064.
25. **Hu, J., and C. Seeger.** 1997. RNA signals that control DNA replication in hepadnaviruses. Semin. Virol. **8:**205–211.
26. **Hu, J., D. Toft, D. Anselmo, and X. Wang.** 2002. In vitro reconstitution of functional hepadnavirus reverse transcriptase with cellular chaperone proteins. J. Virol. **76:**269–279.
27. **Hu, J., D. O. Toft, and C. Seeger.** 1997. Hepadnavirus assembly and reverse transcription require a multi-component chaperone complex which is incorporated into nucleocapsids. EMBO J. **16:**59–68.
28. **Junker-Niepmann, M., R. Bartenschlager, and H. Schaller.** 1990. A short cis-acting sequence is required for hepatitis B virus pregenome encapsidation and sufficient for packaging of foreign RNA. EMBO J. **9:**3389–3396.
29. **Kornburg, A., and T. A. Baker.** 1992. DNA replication, 2nd ed. Freeman, San Francisco, CA.
30. **Lanford, R. E., Y. H. Kim, H. Lee, L. Notvall, and B. Beames.** 1999. Mapping of the hepatitis B virus reverse transcriptase TP and RT domains by transcomplementation for nucleotide priming and by protein-protein interaction. J. Virol. **73:**1885–1893.
31. **Lanford, R. E., L. Notvall, and B. Beames.** 1995. Nucleotide priming and reverse transcriptase activity of hepatitis B virus polymerase expressed in insect cells. J. Virol. **69:**4431–4439.
32. **Lanford, R. E., L. Notvall, H. Lee, and B. Beames.** 1997. Transcomplementation of nucleotide priming and reverse transcription between independently expressed TP and RT domains of the hepatitis B virus reverse transcriptase. J. Virol. **71:**2996–3004.
33. **Lin, L., and J. Hu.** 2008. Inhibition of hepadnavirus reverse transcriptase-ε RNA interaction by porphyrin compounds. J. Virol. **82:**2305–2312.
34. **Mellors, J. W., H. Z. Bazmi, R. F. Schinazi, B. M. Roy, Y. Hsiou, E. Arnold, J. Weir, and D. L. Mayers.** 1995. Novel mutations in reverse transcriptase of human immunodeficiency virus type 1 reduce susceptibility to foscarnet in laboratory and clinical isolates. Antimicrob. Agents Chemother. **39:**1087–1092.
35. **Pelletier, H., M. R. Sawaya, W. Wolfle, S. H. Wilson, and J. Kraut.** 1996. A structural basis for metal ion mutagenicity and nucleotide selectivity in human DNA polymerase beta. Biochemistry **35:**12762–12777.
36. **Pollack, J. R., and D. Ganem.** 1994. Site-specific RNA binding by a hepatitis B virus reverse transcriptase initiates two distinct reactions: RNA packaging and DNA synthesis. J. Virol. **68:**5579–5587.
37. **Radziwill, G., W. Tucker, and H. Schaller.** 1990. Mutational analysis of the

hepatitis B virus P gene product: domain structure and RNase H activity. J. Virol. **64:**613–620.
38. **Ranjith-Kumar, C. T., Y. C. Kim, L. Gutshall, C. Silverman, S. Khandekar, R. T. Sarisky, and C. C. Kao.** 2002. Mechanism of de novo initiation by the hepatitis C virus RNA-dependent RNA polymerase: role of divalent metals. J. Virol. **76:**12513–12525.
39. **Salas, M.** 1991. Protein-priming of DNA replication. Annu. Rev. Biochem. **60:**39–71.
40. **Seeger, C., and J. Hu.** 1997. Why are hepadnaviruses DNA and not RNA viruses? Trends Microbiol. **5:**447–450.
41. **Seeger, C., E. H. Leber, L. K. Wiens, and J. Hu.** 1996. Mutagenesis of a hepatitis B virus reverse transcriptase yields temperature-sensitive virus. Virology **222:**430–439.
42. **Seeger, C., F. Zoulim, and W. S. Mason.** 2007. Hepadnaviruses, p. 2977–3030. *In* D. M. Knipe and P. M. Howley (ed.), Fields virology. Lippincott, Williams & Wilkins, Philadelphia, PA.
43. **Stahl, M., J. Beck, and M. Nassal.** 2007. Chaperones activate hepadnavirus reverse transcriptase by transiently exposing a C-proximal region in the terminal protein domain that contributes to epsilon RNA binding. J. Virol. **81:**13354–13364.
44. **Staschke, K. A., and J. M. Colacino.** 1994. Priming of duck hepatitis B virus reverse transcription in vitro: premature termination of primer DNA induced by the 5′-triphophate of fialuridine. J. Virol. **68:**8265–8269.
45. **Summers, J., and W. S. Mason.** 1982. Replication of the genome of a hepatitis B-like virus by reverse transcription of an RNA intermediate. Cell **29:**403–415.
46. **Tachedjian, G., D. J. Hooker, A. D. Gurusinghe, H. Bazmi, N. J. Deacon, J. Mellors, C. Birch, and J. Mills.** 1995. Characterisation of foscarnet-resistant strains of human immunodeficiency virus type 1. Virology **212:**58–68.
47. **Tavis, J. E., and D. Ganem.** 1996. Evidence for activation of the hepatitis B virus polymerase by binding of its RNA template. J. Virol. **70:**5741–5750.
48. **Tavis, J. E., B. Massey, and Y. Gong.** 1998. The duck hepatitis B virus polymerase is activated by its RNA packaging signal, epsilon. J. Virol. **72:**5789–5796.
49. **Tavis, J. E., S. Perri, and D. Ganem.** 1994. Hepadnavirus reverse transcription initiates within the stem-loop of the RNA packaging signal and employs a novel strand transfer. J. Virol. **68:**3536–3543.
50. **Urban, M., D. J. McMillan, G. Canning, A. Newell, E. Brown, J. S. Mills, and R. Jupp.** 1998. In vitro activity of hepatitis B virus polymerase: requirement for distinct metal ions and the viral epsilon stem-loop. J. Gen. Virol. **79:**1121–1131.
51. **Wang, G. H., and C. Seeger.** 1993. Novel mechanism for reverse transcription in hepatitis B viruses. J. Virol. **67:**6507–6512.
52. **Wang, G. H., and C. Seeger.** 1992. The reverse transcriptase of hepatitis B virus acts as a protein primer for viral DNA synthesis. Cell **71:**663–670.
53. **Wang, G. H., F. Zoulim, E. H. Leber, J. Kitson, and C. Seeger.** 1994. Role of RNA in enzymatic activity of the reverse transcriptase of hepatitis B viruses. J. Virol. **68:**8437–8442.
54. **Wang, X., and J. Hu.** 2002. Distinct requirement for two stages of protein-primed initiation of reverse transcription in hepadnaviruses. J. Virol. **76:**5857–5865.
55. **Wang, X., X. Qian, H.-C. Guo, and J. Hu.** 2003. Heat shock protein 90-independent activation of truncated hepadnavirus reverse transcriptase. J. Virol. **77:**4471–4480.
56. **Weber, M., V. Bronsema, H. Bartos, A. Bosserhoff, R. Bartenschlager, and H. Schaller.** 1994. Hepadnavirus P protein utilizes a tyrosine residue in the TP domain to prime reverse transcription. J. Virol. **68:**2994–2999.
57. **Zhang, Z., and J. E. Tavis.** 2006. The duck hepatitis B virus reverse transcriptase functions as a full-length monomer. J. Biol. Chem. **281:**35794–35801.
58. **Zoulim, F., and C. Seeger.** 1994. Reverse transcription in hepatitis B viruses is primed by a tyrosine residue of the polymerase. J. Virol. **68:**6–13.